Analytical model for the capacity of compressive arch action of reinforced concrete sub-assemblages

Yu, Jun; Tan, Kang Hai

2014

Yu, J., & Tan, K. H. (2014). Analytical model for the capacity of compressive arch action of reinforced concrete sub-assemblages. Magazine of concrete research, 66(3), 109-126.

https://hdl.handle.net/10356/101021

https://doi.org/10.1680/macr.13.00217

Magazine of Concrete Research
Volume 66 Issue 3

Analytical model for the capacity of compressive arch action of reinforced concrete sub-assemblages
Yu and Tan

Magazine of Concrete Research, 2014, **66**(3), 109–126
http://dx.doi.org/10.1680/macr.13.00217
Paper 1300217
Received 24/07/2013; revised 16/10/2013; accepted 17/10/2013
Published online ahead of print 13/12/2013

ice
Institution of Civil Engineers
publishing

Analytical model for the capacity of compressive arch action of reinforced concrete sub-assemblages

Jun Yu
Associate Professor, College of Civil and Transportation Engineering, Hohai University, Nanjing, China

Kang Hai Tan
Professor, School of Civil & Environmental Engineering, Nanyang Technological University, Singapore

Compressive arch action (CAA) is a favourable structural mechanism to mitigate progressive collapse of reinforced concrete (RC) frames. To quickly and accurately predict the CAA capacity of RC sub-assemblages under a column-missing scenario, an engineering analytical model is proposed. The model considers all the design parameters in beams and the imperfect boundary conditions of sub-assemblages, including partial axial and rotational restraints, and connection gaps at beam ends if any. The proposed model is then validated with experimental results and extended to calculate progressive collapse resistance due to CAA with dynamic increase factors. Finally, the model is employed in parametric studies. It is found that CAA capacity increases with restraint stiffness only in the regime of weak restraints; in the regime of strong restraints, CAA capacity is not sensitive to variation in restraint stiffness. Furthermore, CAA enhances structural resistance more evidently for sub-assemblages with small span-to-depth ratios and low mechanical reinforcement ratios, and RC slabs help to increase the CAA capacities of RC frames.

Notation

A	cross-sectional area of beam sections
A_s, A'_s	area of tensile and compression reinforcement
a_{s1}, a_s	distance from the utmost tension fibre of concrete to the centroid of tension reinforcement at the beam ends and the middle joint interfaces respectively
a'_{s1}, a'_s	distance from the extreme compression fibre of concrete to the centroid of compression reinforcement at the beam ends and at the joint interfaces respectively
b	width of beam section
b_j	middle joint width
C'_c, C_c	concrete compressive forces acting at the beam ends and the joint interfaces respectively
C'_s, C_s	steel compressive forces acting at the beam ends and the joint interfaces respectively
c, c_1	neutral-axis depth at joint interfaces and beam ends respectively
E_c	elastic modulus of concrete
E_s	elastic modulus of steel reinforcement
f_c'	compressive strength of concrete
f_y	yield strength of reinforcement
h	depth of beam section
K_a, K_r	stiffness of axial and rotational restraints respectively
k_{eq}	equivalent axial restraint stiffness at beam ends
k_1, k_2	actual axial restraint stiffness at beam ends
l	total net span length of the two-bay beam
l_n	net span length of a one-bay beam
l_1	distance from the top fibre at the beam end to the original support
M	bending moment acting at a beam section
M_n, M_{n1}	nominal moments of resistance of the joint interface and the beam end respectively
M_u, M_{u1}	bending moments acting at the joint interface and the beam end respectively
N	axial force acting at a beam section
N_{max}	maximum axial compression used for comparison reference
N_u, N_{u1}	axial force acting at the joint interfaces and the beam ends respectively
P	vertical resistance of sub-assemblages (or beams) subjected to a concentrated load
P_a	compressive arch action capacity of sub-assemblages
P_f	flexural capacity of sub-assemblages
P_{tot}	vertical resistance of sub-assemblages (or beams) subjected to a uniformly distributed load
q	uniformly distributed load
T', T	steel tensile forces acting at beam ends and joint interfaces respectively
t	lateral deformation of the axial restraint
t_0	gap between axial restraints and beam ends
V	shear force acting at the middle joint interface
β	ratio of l_n to l

β_1	ratio of the equivalent rectangular stress block depth to the neutral-axis depth
γ_a, γ_r	relative axial and rotational restraint stiffness at beam ends respectively
Δ	displacement of the equivalent axial restraint at beam ends
Δ_1, Δ_2	displacements of actual axial restraint at beam ends
δ	beam deflection or displacement at the middle joint
ε	uniform axial strain throughout the two-bay beam
ε_{cu}	ultimate compressive strain of concrete, assumed to be 0·003
ε_s, ε'_s	strain of tension and compression reinforcement
ε_y	yield strain of steel reinforcement
θ	rotation of the lateral support at the beam end
ρ	flexural reinforcement ratio
ϕ	beam end rotation with respect to the rotated support
ω	mechanical reinforcement ratio

Introduction

The alternate load path (ALP) method is one of the direct design approaches to evaluate structural resistance against progressive collapse of buildings by introducing column-removal scenarios (US DoD, 2010; GSA, 2003). Accordingly, several research groups (FarhangVesali *et al.*, 2013; Sasani and Kropelnicki, 2008; Su *et al.*, 2009; Yu and Tan, 2013a, 2013b) have experimentally studied the structural behaviour of reinforced concrete (RC) sub-assemblages under middle column removal scenarios. The test results (Su *et al.*, 2009; Yu and Tan, 2013a, 2013b) indicate that compressive arch action (CAA) can substantially increase the structural resistance of RC frames beyond flexural capacity, which ignores the presence of beam axial compression. Moreover, sub-assemblage deflections corresponding to CAA capacities of, say, around 0·16–0·34 beam depth in the tests of Su *et al.* and around 0·18–0·46 beam depth in the work of Yu and Tan were much smaller than those for catenary action capacities (typically greater than one beam depth). CAA is thus a favourable ALP as it can be mobilised at much smaller deflections.

In practice, ALP analysis is conducted to determine whether progressive collapse can be prevented within specified deformation limits such as the acceptance criteria in UFC 4-023-03 (US DoD, 2010). That is, large structural resistance has to be achieved within limited deformation. Structural performance at the CAA stage fits into this framework. Currently, CAA can be numerically analysed with relatively advanced techniques, such as by introducing fibre plastic hinges at critical sections (Sasani *et al.*, 2011) or by using fibre-based beam elements for all beams (Yu and Tan, 2013a). However, both fibre-based hinges and beam elements require detailed characterisations of material properties of concrete and reinforcement, which have to be assumed at the design stage. Also, the estimation of plastic hinge length in using fibre-based hinges may introduce additional inaccuracy in predicting structural deformation. If CAA capacity is of primary interest, engineering analytical approaches can be used instead, and these can be programmed into Excel spreadsheets. The model of Park and Gamble (2000) is a good method to estimate the compressive membrane action (CMA) capacity of lateral-edge-restrained RC slabs. Due to the similarity of CMA and CAA, the Park and Gamble model can also be used for calculating CAA capacities. However, the model needs to assume the stress state of compression reinforcement at the beam critical sections as either attaining yield strength or having zero stress, which violates the test findings that compression reinforcement at the middle joint regions could either be in yield or in an elastic state (Yu and Tan, 2010). In addition, the Park and Gamble model only considers the effect of partial axial restraints at beam ends without considering partial rotational restraints and connection gaps. The latter, in particular, has significant impact on the development of CAA.

To predict the CAA capacity of RC beams more accurately and efficiently, a new engineering analytical model that accounts for the actual stress state of compression reinforcement and all imperfect boundary conditions is proposed. The model simply requires input data of geometrical properties, the design strength of materials and boundary conditions. The proposed model is validated with available test results (FarhangVesali *et al.*, 2013; Sasani and Kropelnicki, 2008; Su *et al.*, 2009; Yu and Tan, 2013a, 2013b). By considering dynamic effects at the CAA stage, CAA capacity can be converted to progressive collapse resistance. Finally, the proposed model is employed to investigate the effects of imperfect boundary conditions, span-to-depth ratios and mechanical reinforcement ratios of beams and RC slabs on CAA capacity.

Development of the analytical model

Force equilibrium

Figure 1(a) shows a beam–column sub-assemblage subjected to a concentrated load with both ends fixed. Due to symmetry, the free body diagrams of a one-bay beam and the middle joint at the CAA stage are shown in Figures 1(b) and 1(c) respectively.

Due to axial restraints at both ends, considerable axial compression is mobilised throughout the beam. At the CAA stage, the rotations of beam sections are small so that there is no appreciable discrepancy between horizontal reaction forces and axial forces in the beam (Yu and Tan, 2013b). Therefore, the axial forces acting at the beam ends (N_{u1}) and the joint interfaces (N_u) are equal

$$N_u = N_{u1} = N \quad (1)$$

Provided that the resistance of the sub-assemblage at shear failure is greater than that at flexural failure, the vertical resistance P is determined based on the moment equilibrium in the one-bay beam as shown in Figure 1(b) and the force equilibrium in the vertical direction at the middle joint as shown in Figure 1(c)

$$P = 2V = 2(M_{u1} + M_u - N\delta - ql_n^2/2)/l_n \quad (2)$$

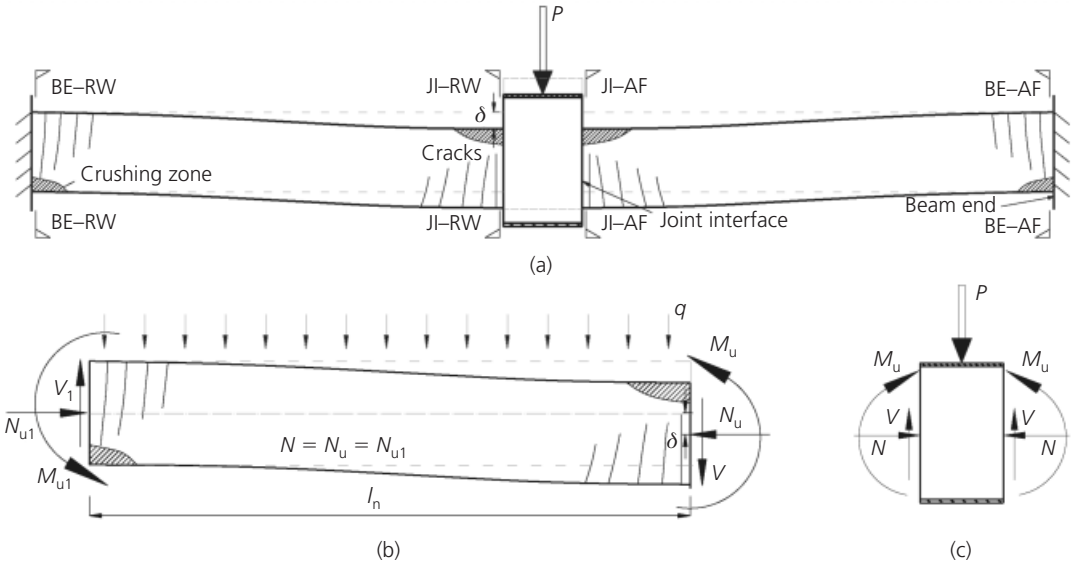

Figure 1. Free body diagrams of RC sub-assemblage at CAA: (a) a beam–column sub-assemblage subjected to a concentrated load; (b) one-bay beam; (c) middle joint

where V is the shear force acting at the middle joint interfaces, M_{u1} and M_u are the ultimate bending moments acting at the beam ends and the joint interfaces respectively, δ is the middle joint displacement, q is the self-weight and l_n is the net span length of a one-bay beam.

If a sub-assemblage is subjected to a uniformly distributed load q, the structural resistance can be determined as

$$P_{tot} = q(2l_n) = 4(M_{u1} + M_u - N\delta)/l_n \quad 3.$$

To determine the P–δ relationship, it is necessary to obtain M–δ and N–δ relationships according to Equation 2 or Equation 3.

Figure 2 shows the experimental and theoretical M–N interaction diagrams at the middle joint interfaces of a typical sub-assemblage specimen S5 (Yu and Tan, 2013b). Negative axial force denotes compression. The theoretical M–N diagrams are computed based on the assumptions that a plane section remains plane and the ultimate strain in the extreme compression fibre of concrete is 0·003 (MacGregor and Wight, 2005), and no strength reduction factor is considered. Curve BD in Figure 2 corresponds to the state that the tension steel has already reached the yield strength when the extreme concrete fibre reaches the ultimate compressive strain of 0·003.

With increasing sub-assemblage deflection, the state of M–N interaction at the joint interface JI–AF (JI denotes joint interface

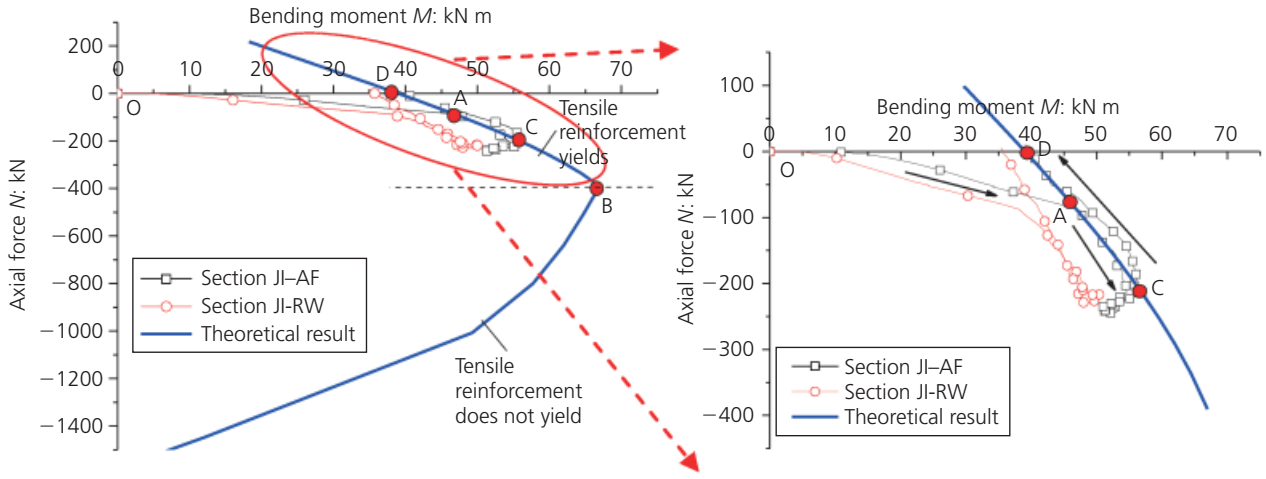

Figure 2. M–N interaction diagram of critical beam sections

and AF denotes the beam end connected to a steel frame) moves from origin O to point A, as shown in Figure 2. Thereafter, the point traverses along the path AC due to the presence of axial compression increasing the ultimate moment of resistance, and then reverses along the path CD after crushing of concrete occurs. The experimental M–N path ACD agrees well with the curve BD of the theoretical M–N diagram. At point A, the ultimate moment of resistance M at section JI–AF is attained, but axial compression has already been mobilised, resulting in an enhanced moment compared to pure flexure at point D. Similar observations can be obtained for the other critical sections indicated in Figure 1(a).

The findings in Figure 2 suggest that, based on theoretical M–N diagrams, both M_u and M_{u1} can be estimated once N is known and, furthermore, P can be determined. Then the kernel of the model is to obtain the N–δ relationship. In the following subsections, the N–δ relationship will be constructed through compatibility conditions and axial force equilibrium of sub-assemblages based on the following assumptions.

Assumptions of the proposed model

The proposed model applies only after plastic hinges have occurred at several critical sections, as shown in Figure 1(a). To compute the cross-sectional forces M and N, the conventional assumptions used in ACI 318-05 (ACI, 2005) are adopted. Namely

(*a*) a plane section remains plane
(*b*) at each critical section, compression concrete has attained its strength with an idealised equivalent rectangular stress block and an ultimate strain of 0·003 in the extreme compression fibre of concrete; tension reinforcement has yielded and concrete tensile strength is ignored.

It is further assumed that

(*c*) the restraints from surrounding structures are converted to equivalent axial and rotational restraints with linear elastic stiffness, as shown in Figure 3.

The spread of failure from the beam above a removed column to surrounding structures is beyond the scope of this paper. Moreover, based on experimental observations (FarhangVesali *et al.*, 2013; Sasani and Kropelnicki, 2008; Su *et al.*, 2009; Yu and Tan, 2013a, 2013b), plastic hinges occur at the beam ends and at the middle joint interfaces, symmetrically located at both sides of the middle joint, as indicated in Figure 3, and the remaining beam segments stay elastic.

The test results (Yu and Tan, 2013b) indicate that axial compression throughout the entire two-bay beam is equal. Due to constant beam cross-sections, axial strains along the elastic beam segments are equal as well. Compared with elastic segments, the plastic hinge lengths and the middle joint width are much smaller, so it is assumed that

(*d*) axial shortening of beams is only induced by elastic axial compressive strains, which are uniform throughout the whole two-bay beam.

According to test results (Yu and Tan, 2010), the strain of compression reinforcement at the CAA stage initially increased up to yielding and subsequently decreased. Thus, it is assumed that

(*e*) the material property of compressive steel reinforcement is elastic–perfectly-plastic, and the unloading slope after yielding equals the initial elastic modulus.

Before a middle column is removed, the bottom reinforcement in the middle joint regions is in elastic compression at service loads. After the column has been removed, the bottom reinforcement is unloaded in compression and reloaded in tension up to yielding. At CAA stage, with increasing middle joint displacement, the tensile strains of the bottom reinforcement keep increasing at the yield plateau with stress equal to the yield strength.

Compatibility conditions

After the ultimate moments of resistance have been obtained at the beam ends and at the joint interfaces, due to symmetry, the deformation and the rotation of one-half of the sub-assemblage are exaggeratedly drawn in Figure 4. Due to mobilisation of axial compression throughout the beam, the deformed beam causes horizontal expansion by amounts $(t + t_0)$ and $0{\cdot}5\varepsilon b_j$ at the lateral support and the middle joint interface respectively. The term t is the small lateral deformation of the axial restraint, equal to $t = N/K_a$, in which N is the induced beam axial compression and

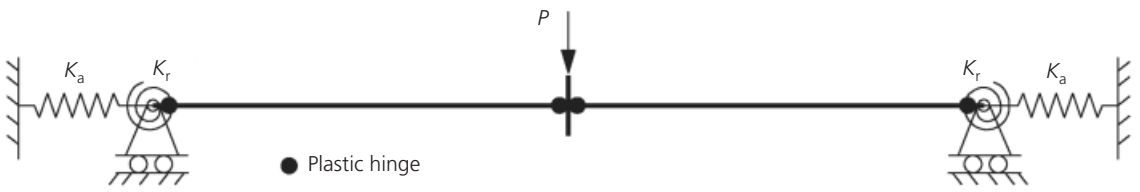

Figure 3. Locations of plastic hinges and equivalent boundary conditions for a two-bay beam

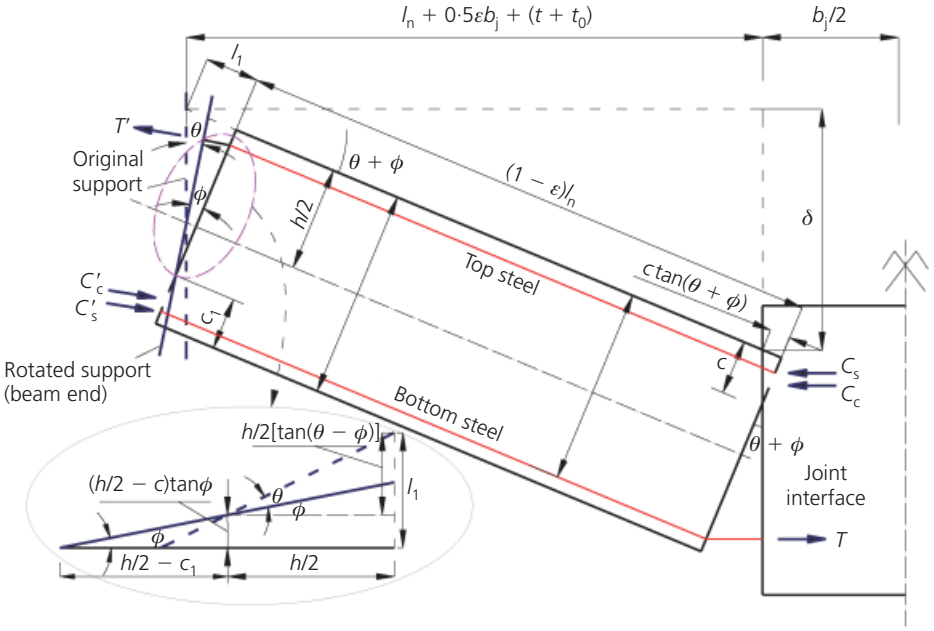

Figure 4. Compatibility conditions of beam–column sub-assemblage

K_a is the axial restraint stiffness. The presence of t_0 (the gap between the support and the beam end) was found in the laboratory tests and is considered in this paper. The term $0{\cdot}5\varepsilon b_j$ represents small axial deformation of the middle joint towards its centre; ε is the uniform axial strain throughout the two-bay beam, equal to $\varepsilon = N/E_cA$ according to assumption (d), b_j is the middle joint width, A is the cross-sectional area of beam sections and E_c is the elastic modulus of concrete.

On the other hand, as shown in Figure 4, a large crack occurs at the beam end with a distance l_1 from the top fibre at the beam end to the original support, and crushing of concrete with a length of $c\tan(\theta + \phi)$ happens at the middle joint interface, in which θ is the rotation of the lateral support at the beam end and ϕ is the beam end rotation with respect to the rotated support. Axial compression in the beam results in an elastic contraction of εl_n along the axis of the deformed beam according to assumption (d), in which l_n is the net span length of the single-bay beam. As shown in Figure 4, the projection of the displaced beam segment onto the original beam configuration yields the compatibility equation

$$[l_n + 0{\cdot}5\varepsilon b_j + (t + t_0)]\sec(\phi + \theta)$$
$$= l_1 + (1 - \varepsilon)l_n - c\tan(\phi + \theta) \quad \text{4a.}$$

The total net span length of the two-bay beam is $l = 2l_n + b_j$. If the ratio l_n/l is denoted as β, the joint width b_j can be expressed as $(1 - 2\beta)l$ and Equation 4a can be converted into

$$[\beta l + 0{\cdot}5\varepsilon(1 - 2\beta)l + (t + t_0)]\sec(\phi + \theta)$$
$$= l_1 + (1 - \varepsilon)\beta l - c\tan(\phi + \theta) \quad \text{4b.}$$

According to the geometric relationships at the beam end restrained by the external support, as illustrated in the inset in Figure 4, the distance l_1 from the top fibre at the beam end to the original support is given by

$$l_1 = h/2[\tan(\phi + \theta)] + (h/2 - c_1)\tan\phi \quad \text{5.}$$

where c_1 is the neutral-axis depth at the beam end.

Substituting Equation 5 into Equation 4b yields the expression for the neutral-axis depth c at the middle joint interface

$$c = \frac{h}{2} - \frac{0{\cdot}5\varepsilon l + (t + t_0)}{\sin(\phi + \theta)} - (1 - \varepsilon)\beta l\frac{2\sin^2[(\phi + \theta)/2]}{\sin(\phi + \theta)} + \left(\frac{h}{2} - c_1\right)\frac{\tan\phi}{\tan(\phi + \theta)} \quad \text{6.}$$

The detailed derivation of Equation 6 from Equations 4 and 5 is shown in Appendix 1.

Since the partial rotational restraint at the beam ends is assumed as a linear elastic spring with a stiffness K_r, when the bending moment M_{u1} acts at the beam end, the corresponding rotation of the lateral support θ can be obtained as

$$\theta = M_{u1}/K_r \quad (7)$$

Substituting the expressions for beam axial strain ε, the axial restraint movement t and Equation 7 into Equation 6 gives

$$c = \frac{h}{2} - \frac{\delta}{2} - \frac{\beta l^2}{2\delta}\left(\frac{1}{E_c A} + \frac{2}{l K_a}\right) N - \frac{\beta l t_0}{\delta} + \left(\frac{h}{2} - c_1\right)\left(1 - \frac{M_{u1}\beta l}{K_r \delta}\right) \quad (8)$$

The derivation of Equation 8 is detailed in Appendix 1.

Equation 8 suggests that c can be expressed as a function of c_1 and δ as both N and M_{u1} can also be determined by c_1, which will be explained later. Thus, for a given vertical displacement δ of the middle joint, c becomes a function of a single variable c_1. To solve the two unknowns c and c_1, one more equation correlating them should be provided.

Determination of beam cross-sectional forces

Based on assumptions (*a*) and (*b*), the stress and strain distributions as well as internal force components at a beam section are shown in Figure 5. Both M and N are calculated with respect to the middle-depth axis of a beam section.

Figure 5(d) shows that the beam axial force is contributed by concrete and reinforcement. Therefore

$$N_{u1} = C'_c + C'_s - T' \quad (9)$$

$$N_u = C_c + C_s - T \quad (10)$$

where C'_c and C_c are the concrete compressive forces, C'_s and C_s the steel compressive forces, and T' and T the steel tensile forces acting on the beam ends and the middle joint interfaces respectively.

Based on Figure 5(c), C'_c can be calculated as

$$C'_c = 0{\cdot}85 f_c' b \beta_1 c_1 \quad (11)$$

where f_c' is the compressive strength of concrete and β_1 is the ratio of the equivalent rectangular stress block depth to the neutral-axis depth, as defined in ACI 318-05 (ACI, 2005).

According to Figure 5(b), the strains of compression and tension reinforcement at the beam ends are given by

$$\varepsilon'_s = (1 - a'_{s1}/c_1)\varepsilon_{cu} \quad (12)$$

$$\varepsilon_s = [(h - a_{s1})/c_1 - 1]\varepsilon_{cu} \quad (13)$$

where a'_{s1} is the distance from the extreme compression fibre of concrete to the centroid of compression reinforcement, a_{s1} is the distance from the utmost tension fibre of concrete to the centroid of tension reinforcement at the beam end and ε_{cu} is a specified ultimate compressive strain of concrete.

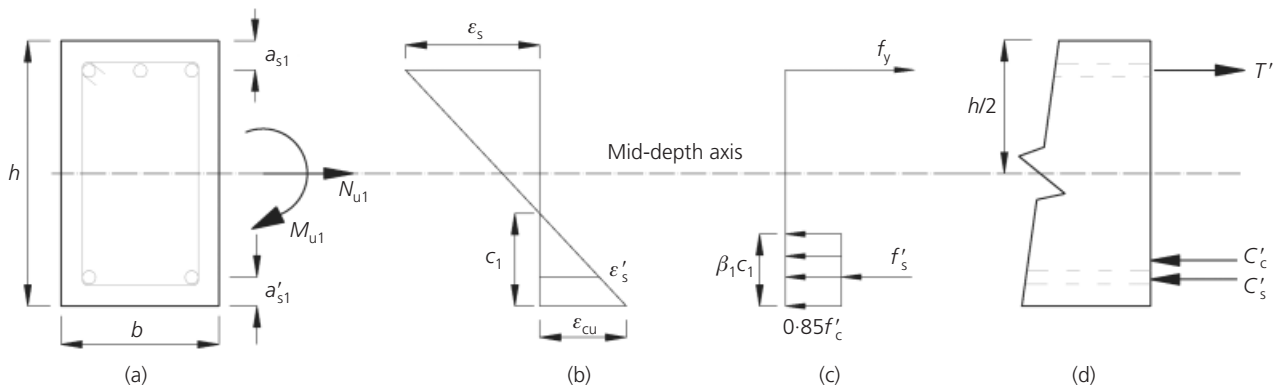

Figure 5. Strain and stress distribution at a beam section: (a) section and forces; (b) strain distribution; (c) stress distribution; (d) internal forces

After obtaining ε'_s via Equation 12, except for the first load step, the strain at each load step should be compared with the one at the last step to check whether compression reinforcement is unloaded. Accordingly, the steel compressive force is determined according to a perfectly-elastic–plastic constitutive model

$$C'_s = \begin{cases} \varepsilon'_s E_s A' & \text{if } \varepsilon'_s < \varepsilon_y \\ f_y A'_s & \text{if } \varepsilon'_s \geqslant \varepsilon_y \text{ and } \varepsilon' \geqslant \varepsilon'_{sp} \\ [f_y - E_s(\varepsilon'_{sp} - \varepsilon'_s)]A_s & \text{if } \varepsilon'_s \geqslant \varepsilon_y \text{ and } \varepsilon' < \varepsilon'_{sp} \end{cases} \quad (14)$$

where ε_y is the yield strain, ε'_{sp} is the strain at the last load step and A'_s is the bar area.

Since the tension reinforcement at the beam end is yielded and the tensile strain keeps increasing at the CAA stage, the corresponding tension is calculated as

$$T' = f_y A_s \quad (15)$$

Due to the reinforcement yielded in tension, ε_s is greater than ε_y. According to Equation 13, c_1 should be less than $c_{yt1} = (h - a_{s1})/(1 + \varepsilon_y/\varepsilon_{cu})$. Likewise, the compressive force of concrete (C_c), the compressive (C_s) and the tensile forces (T) of reinforcement at the joint interfaces can be determined from Equations 11 to 15, but as functions of the neutral-axis depth c. Finally, according to Figure 5(d), the bending moments M_{u1} and M_u at the beam ends and the joint interfaces can be determined with respect to mid-depth axis as

$$M_{u1} = C'_c(h/2 - \beta_1 c_1/2) + C'_s(h/2 - a'_{s1}) + T'(h/2 - a_{s1}) \quad (16)$$

$$M_u = C_c(h/2 - \beta_1 c/2) + C_s(h/2 - a'_s) + T(h/2 - a_s) \quad (17)$$

where a'_s and a_s are the counterparts at the middle joint interface to a'_{s1} and a_{s1} respectively, as shown in Figure 5(a).

In summary, Equations 9 to 17 show that N_u and N_{u1} are functions of c and c_1 respectively, and the equilibrium of axial force in Equation 1 correlates c with c_1. In other words, c is a function of c_1. Note that if the effects of slabs are considered, beam sections will become T- or L-shaped, and then the determination of internal forces should be slightly modified only when the flanges are under compression.

Implementation of the model

Axial force equilibrium gives one equation in terms of the two unknowns c and c_1, independent of δ, and the compatibility condition produces the second equation (i.e. Equation 8) in terms of c, c_1 and δ. Consequently, for a given δ, solving these two non-linear equations simultaneously can determine the values of c and c_1. Subsequently, by substituting c and c_1 into Equations 9 to 17, one can obtain the axial force N and bending moments M_{u1} and M_u and, furthermore, determine the vertical resistance P according to Equation 2 or 3. It is tedious to express these two non-linear equations explicitly. However, by following the procedure shown in Figure 6 and gradually increasing δ, CAA capacity and the maximum beam compression force can be obtained. Implementation of this proposed model can be achieved using either the Matlab program or Excel spreadsheets. In the procedure, two points should be noted.

- Determine the upper bound value (denoted $c_{1\text{-upp}}$) of the neutral-axis depth c_1 at the beam end to ensure that the neutral-axis depth c at the middle joint interface is greater than zero via Equation 8 and tension reinforcement is at yield stage.
- Solve c_1 in an interval between $0{\cdot}01c_{yt1}$ and $c_{1\text{-upp}}$. If there is no solution in this interval, calculation should be stopped and P_{max} and N_{max} can be selected from the previous load steps.

Equivalent stiffness of restraints

When restraints from the surrounding structures to a beam–column sub-assemblage are converted to equivalent restraints as shown in Figure 3, it is very likely that the restraint stiffnesses at the two ends of a sub-assemblage are unequal. For example, the axial restraint stiffnesses are k_1 and k_2 at each end of the sub-assemblage, and the corresponding displacements are Δ_1 and Δ_2 respectively under a given load. The equivalent symmetrical axial restraints must satisfy force equilibrium and deformation compatibility caused by the actual axial restraints at both ends. Therefore

$$k_1\Delta_1 = k_2\Delta_2 = k_{eq}\Delta \quad (18)$$

$$2\Delta = \Delta_1 + \Delta_2 \quad (19)$$

Combining Equation 18 with Equation 19 gives the equivalent axial stiffness k_{eq}, which satisfies assumption (c)

$$k_{eq} = 2k_1k_2/(k_1 + k_2) \quad (20)$$

where Δ is the displacement of equivalent axial restraints.

If a sub-assemblage is simply supported at both ends, either k_1 or k_2 equals zero. As a result, k_{eq} is zero according to Equation 20. As shown by Equation 8, the value of neutral-axis depth c at the joint interfaces will tend to negative infinity; that is, no

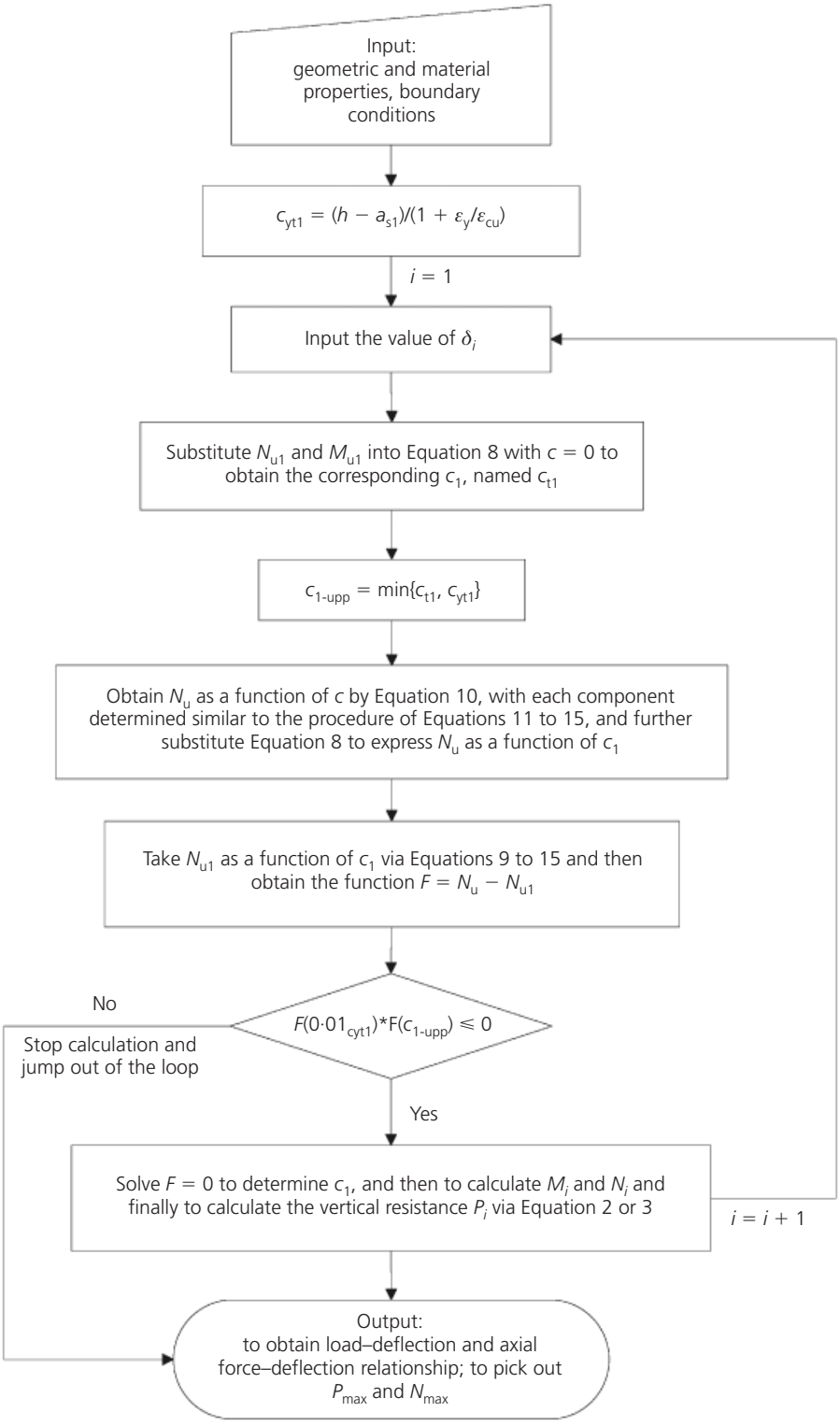

Figure 6. Procedure for calculation of vertical resistance and internal force

compression zone at the middle joint interfaces. Therefore, CAA cannot be mobilised.

The equivalent rotational stiffness is simply selected as the smaller stiffness of both ends because the weaker rotational restraint significantly reduces compression zone at the beam ends.

Validation of the proposed model

A comparison of experimental and analytical results is given in Table 1. Similar to the test results, the proposed model does not consider the effect of the self-weight of specimens. The geometric and material properties of all the specimens and associated boundary conditions are also included in Table 1. More detailed information about the tests can be found in the corresponding papers (FarhangVesali *et al.*, 2013; Sasani and Kropelnicki, 2008; Su *et al.*, 2009; Yu and Tan, 2013a, 2013b). Since the restraint stiffnesses and the maximum axial force in the test of Sasani and Kropelnicki (2008) were not provided, large restraint stiffnesses are assumed in the analysis and the corresponding maximum axial force is not used for comparison. Similarly, a large axial restraint stiffness of $1{\cdot}0 \times 10^6$ kN/m was assumed in the tests reported by FarhangVesali *et al.* (2013) and the corresponding predicted axial forces were not compared. The comparisons in Table 1 indicate that the proposed analytical model is able to predict the capacity of CAA and the maximum beam axial compression with satisfactory accuracy and reliability. For predicting CAA capacity, the mean value is 0·965 and the coefficient of variation (CoV) is less than 10%.

Figure 7 shows that the proposed model can also predict the reasonable trend of load–deflection (P–δ) and beam axial force–deflection (N–δ) relationships of the sub-assemblages, from the deflection of one-tenth to one beam depth. Compared with the experimental results, the proposed model tends to predict smaller displacements corresponding to the CAA capacity; this is due to ignoring the flexural deformation of elastic beam segments and the possible fixed-end rotation due to bar slips. In addition, the model can only be applied with sufficient vertical deflection when plastic hinges have developed at all critical sections. However, when a sub-assemblage deflects beyond one beam depth, it is likely that catenary action takes over CAA to sustain applied loads. Therefore, the P–δ and N–δ relationships are discussed within the deflection range of one-tenth to one beam depth.

Dynamic increase factors at CAA stage

To assess progressive collapse resistance, dynamic effects must be considered. According to the non-linear static analysis with the ALP method in UFC 4-023-03 (US DoD, 2010), dynamic effects can be incorporated by using dynamic increase factors (DIFs). Progressive collapse resistance is equal to static resistance divided by a corresponding DIF. The DIF model in UFC 4-023-03 (Figure 8) is derived from curve fitting on elastic–plastic hardening structural responses. The DIF decreases with increasing the ratio of plastic to yield rotations (or ductility). Because the structural behaviour of an RC sub-assemblage from the elastic state to the CAA capacity presents an elastic–plastic hardening performance, the DIF model shown in Figure 8 can be used to estimate DIFs at CAA capacities.

Since the deflections corresponding to CAA capacities predicted by the proposed model are always smaller than those found in the tests, the experimental results were used to determine DIFs at CAA capacities, as shown in Table 2. More information about each specimen is given in Table 1. The total rotation at CAA capacity is determined by chord rotation, as recommended in UFC 4-023-03. The approach to calculate the yield rotation is illustrated in Appendix 2. The difference between the chord rotation and the yield rotation is the plastic rotation. Table 2 shows that the DIFs are less than 1·15 at CAA capacities for all sub-assemblages. Moreover, Figure 8 shows that the decrement of DIF is not significant when the ratio $\theta_{pra}/\theta_y > 4$. For conservatism, the value of 1·15 is suggested as the DIF for analysis on CAA. That is, progressive collapse resistance is around 87% of the corresponding calculated CAA capacity.

Parametric studies on CAA capacities

Under a middle column removal scenario, CAA is mobilised because adequate horizontal restraints are provided to allow the development of axial force. However, under a penultimate or a corner column removal scenario, the main structural mechanism to redistribute gravity loads is essentially a flexural mechanism of beams without axial force (Sasani and Sagiroglu, 2008). Therefore, the development of CAA is significantly affected by boundary conditions, which can be converted to axial, rotational and vertical supports at beam ends, as illustrated in Figure 3. Moreover, in practice, the geometric and material properties of beams vary over a large range. All these parameters may affect the development of CAA. Therefore, the proposed analytical model was used to investigate the effects of imperfect boundary conditions, reinforcement ratios of beams, beam span-to-depth ratios and RC slabs on the development of CAA.

Effect of axial connection gaps

As with the laboratory testing, it was found that connection gaps existed between boundary restraints and specimens. Because hole tolerance is required to facilitate installing and dismantling a specimen before and after testing, connection gaps are inevitable. However, in cast-in-situ RC structures, there is no gap in continuous beams. Therefore, specimen S4, with parameters shown in Table 1, was used to investigate the effect of axial connection gaps on CAA capacities.

Figure 9 shows that the overall trends of the load–deflection relationships are similar under different connection gaps. CAA resistance is normalised by CAA capacity P_0 at zero gap (i.e. $t_0 = 0$). Compared with a total beam span length of 5750 mm, a gap of 0·8 mm is negligible. However, when the gap increases by 0·8 mm, the CAA capacity P_a of the sub-assemblage decreases by around 8%, indicating that CAA capacity is very sensitive to axial connection gaps. Therefore, it is necessary to measure the

Test[a]	Boundary conditions			Beam sections		l/h[b]	Longitudinal reinforcement at middle joints[c]		Material properties		Capacity of CAA: kN			Maximum axial compression: kN		
	Axial stiffness: kN/m	Axial gap: mm	Rotational stiffness: kNm/rad	Width b: mm	Depth h: mm		Top	Bottom	f_c': MPa	f_y: MPa	Test P_u	Analytical P_a	P_a/P_u	Test N_u	Analytical N_a	N_a/N_u
S1	$1{\cdot}06 \times 10^5$	0·5	$1{\cdot}00 \times 10^4$	150	250	23·0	2T10 + 1T13	2T10	31·24	511	41·64	43·57	1·046	177·9	156·70	0·881
S2	$1{\cdot}06 \times 10^5$	1·2	$1{\cdot}00 \times 10^4$	150	250	23·0	3T10	2T10	31·24	511	38·38	38·39	1·000	155·9	141·86	0·910
S3	$4{\cdot}29 \times 10^5$	1·0	$3{\cdot}00 \times 10^4$	150	250	23·0	3T13	2T10	38·15	511 (T10), 494 (T13)	54·47	56·15	1·031	221·0	227·85	1·031
S4	$4{\cdot}29 \times 10^5$	0·8	$3{\cdot}00 \times 10^4$	150	250	23·0	3T13	2T13	38·15	494	63·22	63·90	1·011	212·7	231·50	1·088
S5	$4{\cdot}29 \times 10^5$	0·8	$3{\cdot}00 \times 10^4$	150	250	23·0	3T13	3T13	38·15	494	70·33	72·16	1·026	238·4	224·03	0·940
S6	$4{\cdot}29 \times 10^5$	0·8	$3{\cdot}00 \times 10^4$	150	250	23·0	3T16	2T13	38·15	494 (T13), 513 (T16)	70·33	74·08	1·053	218·1	196·49	0·901
S7	$4{\cdot}29 \times 10^5$	1·2	$3{\cdot}00 \times 10^4$	150	250	18·2	3T13	2T13	38·15	494	82·82	83·15	1·004	233·1	244·61	1·049
S8	$4{\cdot}29 \times 10^5$	0·8	$3{\cdot}00 \times 10^4$	150	250	13·4	3T13	2T13	38·15	494	121·34	126·31	1·041	272·5	300·15	1·101
A1	$1{\cdot}00 \times 10^6$	0·0	$1{\cdot}75 \times 10^4$	150	300	9·0	2Ø12	2Ø12	24·55	350	168·00	152·53	0·908	388·0	338·71	0·873
A2	$1{\cdot}00 \times 10^6$	0·0	$1{\cdot}75 \times 10^4$	150	300	9·0	3Ø12	3Ø12	26·83	350	221·00	190·04	0·860	324·0	367·68	1·135
A3	$1{\cdot}00 \times 10^6$	0·0	$1{\cdot}75 \times 10^4$	150	300	9·0	3Ø14	3Ø14	29·64	340	246·00	228·34	0·928	305·0	403·08	1·322
A4	$1{\cdot}00 \times 10^6$	0·0	$1{\cdot}75 \times 10^4$	150	300	9·0	2Ø12	1Ø14	21·89	350 (Ø12), 340 (Ø14)	147·00	133·09	0·905	344·0	305·08	0·887
A5	$1{\cdot}00 \times 10^6$	0·0	$1{\cdot}75 \times 10^4$	150	300	9·0	3Ø12	2Ø12	25·16	350	198·00	169·14	0·854	393·0	348·02	0·886
A6	$1{\cdot}00 \times 10^6$	0·0	$1{\cdot}75 \times 10^4$	150	300	9·0	3Ø14	2Ø14	27·21	340	226·00	200·00	0·885	191·0[d]	380·37	—
B1	$1{\cdot}00 \times 10^6$	0·0	$1{\cdot}75 \times 10^4$	150	300	14·0	3Ø14	3Ø14	17·63	340	125·00	111·93	0·895	225·0	230·45	1·024
B2	$1{\cdot}00 \times 10^6$	0·0	$1{\cdot}75 \times 10^4$	150	300	19·0	3Ø14	3Ø14	18·32	340	82·90	79·71	0·962	210·0	222·67	1·060
B3	$1{\cdot}00 \times 10^6$	0·0	$1{\cdot}75 \times 10^4$	150	300	19·0	3Ø14	2Ø14	20·06	340	74·70	72·57	0·971	210·0	244·85	1·166
C1	$1{\cdot}00 \times 10^6$	0·0	$1{\cdot}75 \times 10^4$	100	200	13·5	2Ø12	2Ø12	15·12	350	60·90	49·62	0·815	108·0	90·95	0·842
SS	$1{\cdot}00 \times 10^6$	0·0	$1{\cdot}00 \times 10^4$	170	190	21·9	5D9·5	2D9·5	41·37	516	74·73	79·65	1·066	—	274·00	—
V1	$1{\cdot}00 \times 10^6$	0·0	$1{\cdot}45 \times 10^4$	180	180	24·4	2N10	2N10	30·50	580	40·50	38·50	0·951	—	199·70	—
V2	$1{\cdot}00 \times 10^6$	0·0	$1{\cdot}35 \times 10^4$	180	180	24·4	2N10	2N10	27·00	580	35·70	35·04	0·982	—	171·90	—
V3	$1{\cdot}00 \times 10^6$	0·0	$1{\cdot}85 \times 10^4$	180	180	24·4	2N10	2N10	30·00	580	41·40	38·29	0·925	—	197·08	—
V4	$1{\cdot}00 \times 10^6$	0·0	$1{\cdot}80 \times 10^4$	180	180	24·4	3N10	2N10	26·00	580	40·10	39·93	0·996	—	160·86	—
V5	$1{\cdot}00 \times 10^6$	0·0	$1{\cdot}60 \times 10^4$	180	180	24·4	3N10	2N10	29·50	580	41·60	40·35	0·970	—	178·55	—
V6	$1{\cdot}00 \times 10^6$	0·0	$1{\cdot}45 \times 10^4$	180	180	24·4	3N10	2N10	30·00	580	39·40	40·62	1·031	—	181·58	—
Mean for all specimens													0·965			1·006
CoV for all specimens													0·070			0·132

[a] S1–S8 from Yu and Tan (2013a, 2013b); A1–C1 from Su *et al.* (2009); SS from Sasani and Kropelnicki (2008); V1–V6 from FarhangVesali *et al.* (2013). Concrete strengths in the tests of Su *et al.* are converted from cubic strength to cylinder strength by multiplying 0·76. Elastic modulus of concrete computed based on specifications of ACI 318-05 (ACI, 2005) if not given in the tests.
[b] l is total length of the whole two-bay beam, equal to the summation of two net span lengths of a single-bay beam and a joint width.
[c] T denotes high-strength reinforcement; the numbers after T, Ø, D and N are used to indicate bar diameter in the corresponding references.
[d] This axial force deviates largely from other test results within the same batch, so is not used for comparison.

Table 1. Comparisons of experimental and analytical results

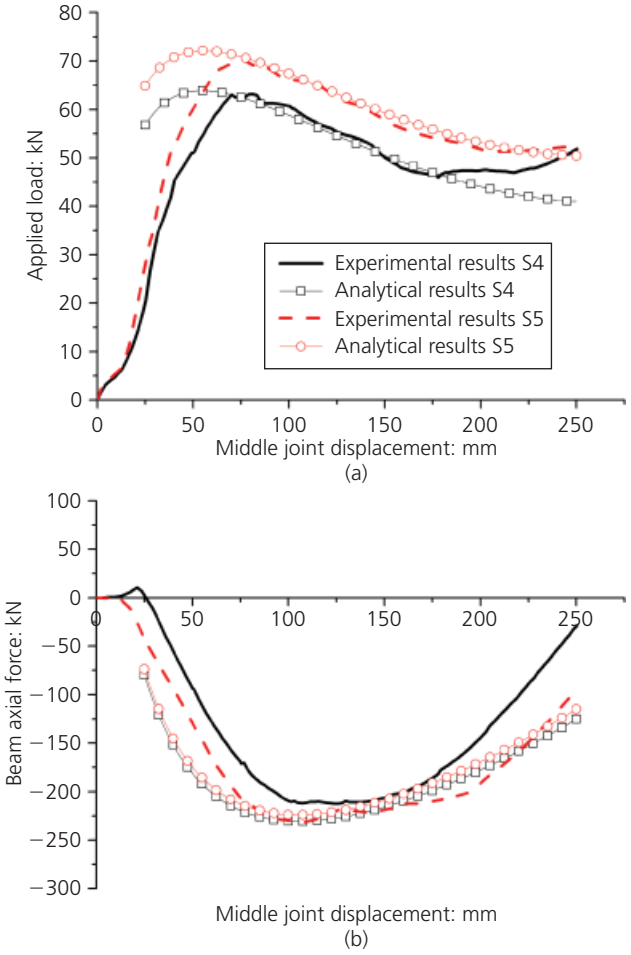

Figure 7. Comparison of experimental and analytical results: (a) load–deflection relationship; (b) axial force–displacement relationship

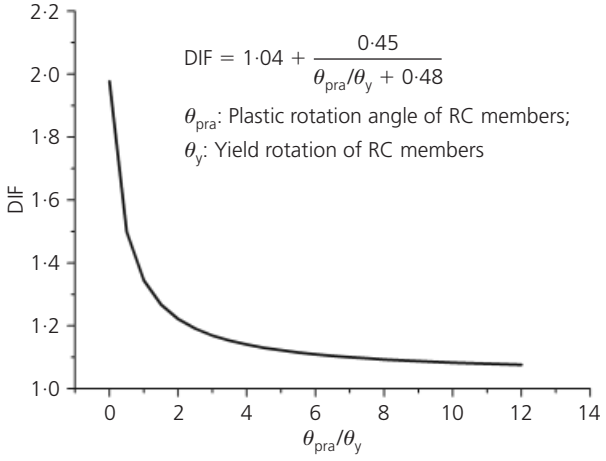

Figure 8. DIF model in UFC 4-023-03 (US DoD, 2010)

gaps between axial restraints and a specimen during testing. Otherwise, the CAA capacity of the specimen will be underestimated compared with its prototype in RC structures. However, this analytical model can be used to re-evaluate P_a of the tested specimens with zero gaps to make the specimens more representative of continuous beams in RC structures.

Effect of axial restraint stiffness

To obtain general conclusions about the effects of partial axial and rotational restraints on CAA capacities, specimens S4, S7 and A5 (Table 1), were selected for parametric study. To illustrate the effect of axial restraint stiffness K_a, the stiffness term is normalised by the beam axial stiffness

$$21. \quad \gamma_a = K_a/(E_c A/l)$$

where γ_a is the non-dimensional relative axial stiffness, E_c is the elastic modulus of concrete, A is the beam cross-sectional area and l is the net span length of the two-bay beam, equal to $2l_n$ plus the column width. For example, for specimen S4, the uncracked beam axial stiffness E_cA/l was $1{\cdot}93 \times 10^5$ kN/m and K_a was $4{\cdot}3 \times 10^5$ kN/m, so $\gamma_a = 2{\cdot}22$. During the analysis, CAA capacities were calculated using different K_a values with zero gap, but the rotational restraint stiffness was kept the same as the one in the tests, as listed in Table 1. The analysis of specimens S7 and A5 followed the same procedure.

To show the beneficial effect of CAA beyond flexural capacity, the CAA capacities P_a were normalised with flexural capacity P_f under a concentrated load. Flexural capacity P_f is calculated by ignoring beam axial force and self-weight in Equation 2 and replacing the ultimate moments (M_u and M_{u1}) with nominal moments of resistance (M_n and M_{n1}). That is

$$22. \quad P_f = 2(M_n + M_{n1})/l_n$$

M_n and M_{n1} are determined without considering strength reduction factors. The flexural capacity of each specimen is shown in Figure 10.

Figure 10 shows that the overall trends of the effect of axial restraint stiffness on CAA capacities are quite similar, although the geometric and material properties of S4, S7 and A5 are quite different. When the axial restraint is weak, defined as $\gamma_a < 1{\cdot}0$, a larger K_a can more effectively increase P_a of each specimen; when the axial restraint is strong, defined as $\gamma_a \geqslant 1{\cdot}0$, K_a does not significantly affect P_a, and the marginal effect of a greater K_a on increasing P_a decreases quickly. For example, from $\gamma_a = 0{\cdot}1$ to $\gamma_a = 1{\cdot}0$, the CAA capacity of S4 increases by around 24%. In contrast, from $\gamma_a = 1{\cdot}0$ to $\gamma_a = 10$, P_a of S4 only increases by around 12%. When $\gamma_a > 5{\cdot}0$, the effect of K_a on CAA can be neglected since, from $\gamma_a = 5$ to $\gamma_a = 100$ the enhancement of CAA capacity of specimen S4 is only 3·6%.

	Single-bay span: mm (*A*)	Deflection at CAA capacity: mm (*B*)	Chord rotation at CAA capacity: rad (*C*) = (*B*)/(*A*)	Yield rotation: rad (*D*)	Plastic rotation: rad (*E*) = (*C*) − (*D*)	DIF
S1	2750	78·0	0·0284	0·0040	0·0243	1·11
S2	2750	73·0	0·0265	0·0040	0·0225	1·11
S3	2750	74·4	0·0271	0·0036	0·0234	1·10
S4	2750	81·0	0·0295	0·0060	0·0234	1·14
S5	2750	74·5	0·0271	0·0079	0·0192	1·19
S6	2750	114·4	0·0416	0·0060	0·0356	1·11
S7	2150	74·4	0·0346	0·0047	0·0299	1·11
A1	1225	48·0	0·0392	0·0016	0·0376	1·06
A2	1225	56·4	0·0460	0·0023	0·0438	1·06
A3	1225	76·4	0·0624	0·0029	0·0594	1·06
A4	1225	65·0	0·0531	0·0012	0·0519	1·05
A5	1225	70·7	0·0577	0·0016	0·0561	1·05
A6	1225	69·2	0·0565	0·0021	0·0544	1·06
B1	1975	100·0	0·0506	0·0054	0·0452	1·09
B2	2725	102·0	0·0374	0·0074	0·0301	1·14
B3	2725	85·5	0·0314	0·0053	0·0261	1·12
C1	1225	33·7	0·0275	0·0050	0·0226	1·13
SS	2000	41·6	0·0208	0·0033	0·0175	1·12

Table 2. DIFs at CAA capacities

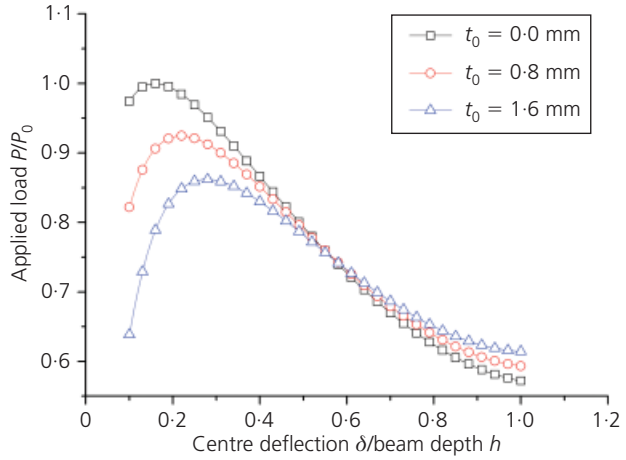

Figure 9. Effect of axial connection gaps on development of CAA (P_0 = 69·10 kN)

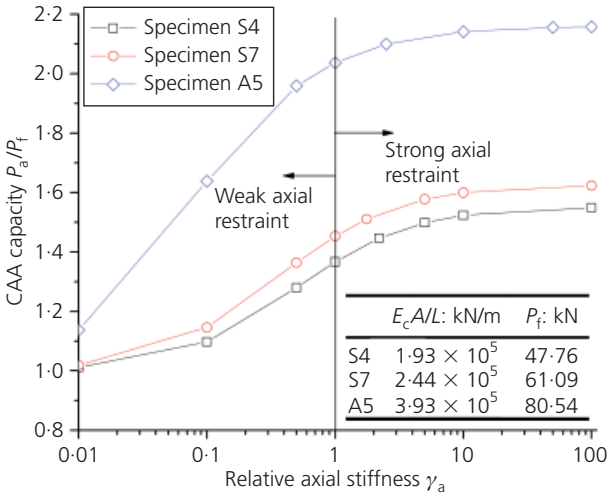

Figure 10. Effect of axial restraint stiffness on CAA capacity

Compared with S4 and S7, the enhancement of structural resistance of A5 due to CAA is more significant, and the CAA capacity of A5 is more sensitive to the variation of axial restraint stiffness in the range $\gamma_a < 1{\cdot}0$. This is mainly attributed to a smaller beam span-to-depth ratio in A5, which will be explained later. Note that in the structural tests (Su *et al.*, 2009; Yu and Tan, 2013b), the provided boundary conditions were regarded as strong axial restraints.

In summary, CAA capacity is sensitive to axial restraint stiffness K_a only when axial restraint is weak (i.e. $\gamma_a < 1{\cdot}0$). The effect of a greater K_a on CAA capacity becomes marginalised when axial restraint is strong (i.e. $\gamma_a \geqslant 1{\cdot}0$). Therefore, to be conservative in design, the beneficial effect of CAA on structural resistance can be considered only when strong axial restraints are provided.

Effect of rotational restraint stiffness

To illustrate the effect of rotational restraint stiffness K_r, this term is normalised by the rotational stiffness of beam ends $4E_cI/l$. Then the relative stiffness γ_r is given by

$$\gamma_r = K_r/(4E_cI/l) \quad (23)$$

where I is the second moment inertia of an uncracked concrete beam section.

For specimen S4, the rotational stiffness of beam ends $4E_cI/l$ was 4028 kN m/rad and K_r was 30 000 kN m/rad, so the corresponding γ_r was 7·4. During the analysis, CAA capacities were calculated using different K_r, but the connection gap was set as zero and the axial restraint stiffness was kept the same as the one in each test, as listed in Table 1. The analysis of S7 and A5 followed the same procedure. Moreover, the CAA capacities were normalised by the corresponding flexural capacities, as indicated in Figure 11.

Figure 11 shows that strong rotational restraint (i.e. $\gamma_r \geqslant 1$) has no significant effect on CAA capacity. For example, from $\gamma_r = 1$ to 5, the increase of CAA capacity of S4 is less than 5%. Moreover, when $\gamma_r \geqslant 5$, the effect of rotational restraint stiffness K_r on P_a can be neglected. However, for weak rotational restraint, defined as $\gamma_r < 1$, P_a decreases significantly with reducing K_r, as large rotations at the beam ends substantially reduce the compressive depth of beam sections. When γ_r is too small (e.g. less than 0·2), CAA cannot be effectively developed for S4.

Similar conclusions about the effect of rotational restraint stiffness K_r can be found in specimens S7 and A5, as illustrated in Figure 11. These help to confirm the experimental finding of Guice and Rhomberg (1988), that high rotational restraint stiffness does not affect the compressive membrane capacity of RC slabs. Therefore, to mobilise CAA, adequate rotational restraints must be provided. To be conservative in design, the provision of strong rotational restraints with $\gamma_r \geqslant 1{\cdot}0$ can be regarded as a prerequisite to include CAA. In the structural tests (Su *et al.*, 2009; Yu and Tan, 2013b), the provided boundary conditions were regarded as strong rotational restraints.

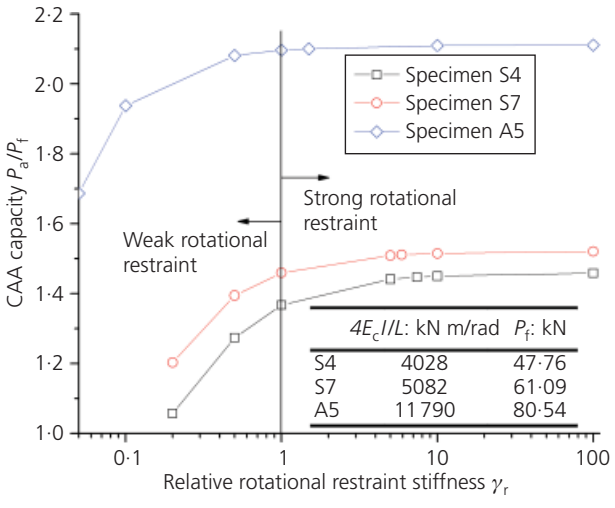

Figure 11. Effect of rotational restraint stiffness on CAA capacity

Effects of beam span-to-depth ratio and mechanical reinforcement ratio

Su *et al.* (2009) reported that CAA capacity is a function of the flexural reinforcement ratio (ρ) and the ratio of beam span (l_n) to depth (h). Considering various yield strengths of steel reinforcement (f_y) and compressive strengths of concrete (f_c'), the mechanical reinforcement ratio $\omega = \rho f_y/f_c'$ is a more representative parameter since ω is frequently used as a measure of the flexural behaviour of a beam and incorporates three major variables affecting that behaviour (MacGregor and Wight, 2005). Therefore, the effects of span-to-depth ratio (l_n/h) and mechanical reinforcement ratio (ω) of beams on CAA are investigated here.

Under a middle column removal scenario, plastic hinges occur near the middle joint interfaces and the beam ends of a sub-assemblage, associated with sagging and hogging moments respectively. Under a sagging moment, the top and the bottom reinforcements at the middle joint interfaces are in compression and tension respectively. Moreover, the top compression reinforcement at the middle joint interfaces is the same as the tension reinforcement at the beam ends subjected to a hogging moment. As a result, the total reinforcement at a middle joint interface can represent all flexural (or tension) reinforcement at critical sections of a single-bay beam and the total reinforcement ratio is used to determine ω.

Based on the investigation of imperfect boundary conditions, both the axial and rotational restraints in the tests of Yu and Tan (2013b) were categorised as strong restraints and they were used to investigate the effect of l_n/h and ω on the CAA of RC sub-assemblages. Five case study groups are listed in Table 3. A large range of flexural reinforcement ratio is covered, from 0·49% to 1·87%. The single-bay beam span-to-depth ratio l_n/h varies from 6·5 to 11. Besides the CAA capacity P_a, the flexural action capacity P_f (determined by Equation 22) and the enhancement factor α of structural resistance due to CAA are also listed in Table 3.

Figure 12 shows that the enhancement factor of RC sub-assemblages due to CAA varies from around 30% to 100%. With increasing mechanical reinforcement ratio ω, α significantly decreases for a given l_n/h. In other words, RC beams with low reinforcement ratios can gain a beneficial effect from CAA. For instance, for $l_n/h = 11$, when ω decreases from 35·72% to 16·32%, α increases from 28·2% to 77·4%. For a known ω, a smaller l_n/h results in a greater α. That is, the enhancement of structural resistance due to CAA in a stocky RC beam is more evident. For example, for $\omega = 16{\cdot}32\%$, when l_n/h decreases from 11·0 to 6·5, the corresponding α increases from 77·4% to 98·0%.

l_n/h	Longitudinal reinforcement and ratio at middle joint interfaces[a]		Mechanical reinforcement ratio ω: %	Flexural action capacity P_f: kN	CAA capacity P_a: kN	Enhancement factor α $(= (P_a - P_f)/P_f)$
	Top	Bottom				
11·0	3T10 (0·73%)	2T10 (0·49%)	16·32	30·25	53·65	0·774
	3T13 (1·23%)	2T10 (0·49%)	22·46	40·47	61·29	0·514
	3T13 (1·23%)	2T13 (0·82%)	26·51	47·27	68·50	0·449
	3T13 (1·23%)	3T13 (1·23%)	31·81	55·94	76·69	0·371
	3T16 (1·87%)	2T13 (0·82%)	35·72	61·56	78·94	0·282
9·5	3T10 (0·73%)	2T10 (0·49%)	16·32	35·03	64·31	0·836
	3T13 (1·23%)	2T10 (0·49%)	22·46	46·86	73·09	0·560
	3T13 (1·23%)	2T13 (0·82%)	26·51	54·74	81·50	0·489
	3T13 (1·23%)	3T13 (1·23%)	31·81	64·78	91·00	0·405
	3T16 (1·87%)	2T13 (0·82%)	35·72	71·29	93·38	0·310
8·5	3T10 (0·73%)	2T10 (0·49%)	16·32	39·15	73·64	0·881
	3T13 (1·23%)	2T10 (0·49%)	22·46	52·37	83·41	0·593
	3T13 (1·23%)	2T13 (0·82%)	26·51	61·18	92·86	0·518
	3T13 (1·23%)	3T13 (1·23%)	31·81	72·40	103·49	0·429
	3T16 (1·87%)	2T13 (0·82%)	35·72	79·67	105·98	0·330
7·5	3T10 (0·73%)	2T10 (0·49%)	16·32	44·37	85·59	0·929
	3T13 (1·23%)	2T10 (0·49%)	22·46	59·36	96·61	0·628
	3T13 (1·23%)	2T13 (0·82%)	26·51	69·34	107·39	0·549
	3T13 (1·23%)	3T13 (1·23%)	31·81	82·05	119·46	0·456
	3T16 (1·87%)	2T13 (0·82%)	35·72	90·29	122·08	0·352
6·5	3T10 (0·73%)	2T10 (0·49%)	16·32	51·20	101·38	0·980
	3T13 (1·23%)	2T10 (0·49%)	22·46	68·49	114·07	0·665
	3T13 (1·23%)	2T13 (0·82%)	26·51	80·00	126·57	0·582
	3T13 (1·23%)	3T13 (1·23%)	31·81	94·67	140·54	0·485
	3T16 (1·87%)	2T13 (0·82%)	35·72	104·19	143·34	0·376

[a] $\rho = A_s/bd$; $b = 150$ mm and $d = 215$ mm.

Table 3. Study cases with different beam span-to-depth ratios and mechanical reinforcement ratios. The stiffness of the axial and the rotational restraints and the material properties are the same as the test of Yu and Tan (2013b): $f_c' = 38{\cdot}2$ MPa, $f_y = 511$ MPa for T10, $f_y = 494$ MPa for T13, $f_y = 513$ MPa for T16; $E_s = 200$ GPa for all reinforcements

In contrast, when $\omega = 35{\cdot}72\%$, such a variation in l_n/h only results in α increasing from 28·2% to 37·6%.

In summary, for beams under adequate axial and rotational restraints, a lower mechanical reinforcement ratio and a lower span-to-depth ratio will give rise to a significant enhancement of structural resistance contributed by CAA.

Effects of RC slabs

In monolithic RC cast-in-situ structures, slabs serve as the top flanges of beams due to good structural integrity. Accordingly, interior and perimeter beams will become T- and L-shaped respectively. Moreover, slab reinforcement can also serve as flexural reinforcement of T- or L-beams. Table 4 shows the cases studied for the effects of RC slabs on CAA capacities. Except for the beam cross-sections, all the study cases have the same boundary conditions and material and geometric properties as those of specimen S4, as shown in Table 1. Note that the connection gaps at beam ends are set as zero in the analysis. S4 has a rectangular section of 250 mm by 150 mm. In the other cases in Table 4, the flange width is assumed to be 500 mm and the variables are the flange depth and consideration of whether slab reinforcement is the flexural reinforcement.

Table 4 indicates that, compared with S4, if the slabs function as top flanges only (cases S4-1, S4-2 and S4-5), the flexural capacity is increased by 7·1% whereas the CAA capacity is enhanced by 17·9–19·4%. If the slab reinforcement in the flanges is also included (cases S4-3 and S4-4), both flexural and CAA capacities are greatly increased. However, the contribution to enhancing CAA capacity from the top flanges is more dominant than that from slab reinforcement. For example, with a top flange of 500 mm by 80 mm (i.e. S4-2), CAA capacity increases from 69·10 kN to 82·02 kN. When the slab reinforcement of 4∅6 is

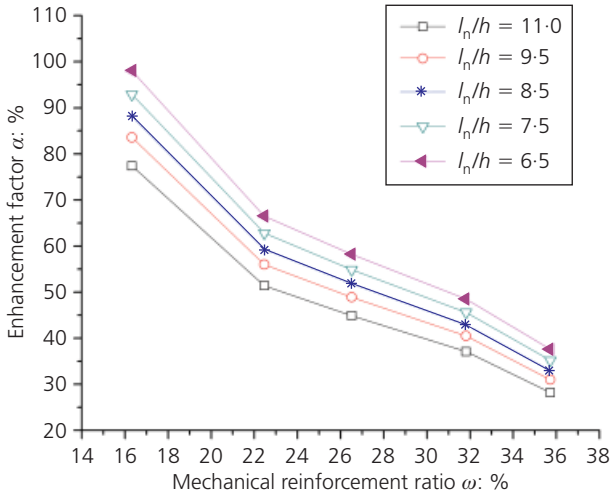

Figure 12. Effect of beam span-to-depth ratio and mechanical reinforcement ratio on CAA capacity

considered (i.e. S4-4), CAA capacity is further increased to 85·83 kN. That is, the slab reinforcement resulted in an additional increment of 3·83 kN (around 5·5% of the CAA capacity of S4). In summary, for analysis of RC frames, it is necessary to consider the beneficial effects of RC slabs on CAA capacity.

Discussion

Although the proposed analytical model is based on RC beam–column sub-assemblages, it can be extended for other scenarios involving the mobilisation of CAA, such as RC columns or masonry walls subjected to impact loads and bridge girders subjected to overload. Moreover, the enhancement factor of structural resistance due to CAA can be incorporated into conventional plastic hinges, as suggested in UFC 4-023-03 (US DoD, 2010), so that the beneficial effect of CAA can be considered in frame analysis and design.

In practice, the two adjacent beams in a sub-assemblage may have unequal spans. In this scenario, the force equilibrium and compatibility equations should be individually established at each single-bay beam. The force equilibrium at the middle joint then links the internal forces (i.e. axial force, bending moment and shear force) in the two single-bay beams. Accordingly, the neutral-axis depths at the two middle joint interfaces and at the two beam ends should be calculated at a given vertical displacement δ of the middle joint. Similar to the procedure shown in Figure 6, load–deflection and axial force–deflection relationships can be obtained. Moreover, the beam with a longer span governs CAA development due to the larger beam span-to-depth ratio reducing the enhancement from CAA. Therefore, the CAA capacity of a sub-assemblage with two unequal-span beams is less than that with two equal-span beams, provided that the total lengths of the two sub-assemblages are the same.

Conclusion

Based on the assumptions commonly used in flexural theory and in the design of RC framed members, an analytical model is proposed to evaluate the CAA of RC beam–column sub-assemblages under a middle column removal scenario, considering the combined effects of stress state of compression reinforcement and imperfect boundary conditions on CAA. The imperfect boundary conditions include partial axial and rotational restraints, and axial connection gaps at beam ends. Comparison of experimental and analytical results indicates that the model is able to predict both the CAA capacity and the maximum beam axial compression of RC sub-assemblages with satisfactory accuracy and reliability. Moreover, the structures present elastic–plastic hardening behaviour at the CAA stage and the DIFs decrease with increasing deformations. Based on available sub-assemblage tests, the DIFs are not greater than 1·15. Therefore, progressive collapse resistance can be estimated as 87% corresponding CAA capacity.

Parametric studies indicate that adequate axial and rotational restraint stiffness must be provided to develop CAA of RC sub-assemblages. When the axial and rotational restraint stiffnesses are respectively greater than those of restrained uncracked beams (i.e. $\gamma_a \geq 1$ and $\gamma_r \geq 1$), the variation of each restraint stiffness

Study case	Top flange: mm	Slab rebar in flange	Flexural capacity P_f: kN	Increase of P_f on top of S4: %	CAA capacity P_a: kN	Increase of P_a on top of S4: %	Beam section (dimensions in mm)
S4	NA[a]	NA	47·27	—	69·10	—	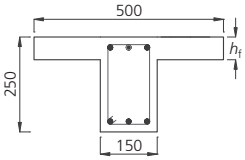
S4-1	60	NA	50·61	7·1	81·46	17·9	
S4-2	80	NA	50·61	7·1	82·02	18·7	
S4-3	80	2Ø6	54·34	15·0	83·96	21·5	
S4-4	80	4Ø6	58·02	22·7	85·83	24·3	
S4-5	100	NA	50·61	8·1	82·49	19·4	

[a] Not available.

Table 4. Effect of RC slabs on CAA capacity

does not significantly affect the CAA capacity of beams. However, when reducing the stiffness of weak restraints ($\gamma_a < 1$ or $\gamma_r < 1$), the CAA capacity will decrease substantially. Therefore, from conservatism, it is suggested that only when both relative axial and rotational stiffness are greater than one (i.e. $\gamma_a \geqslant 1$ and $\gamma_r \geqslant 1$), CAA can be considered as a beneficial alternate load path to mitigate progressive collapse.

The span-to-depth ratio and the mechanical reinforcement ratio of beams are two key parameters affecting CAA capacity. The enhancement of structural resistance due to CAA is highly dependent on different combinations of these two parameters. For beams with adequate axial and rotational restraints as well as shear strength, a lower mechanical reinforcement ratio and a lower span-to-depth ratio will give rise to significant enhancement of structural resistance contributed by CAA. Finally, RC slabs can greatly increase CAA capacities by serving as top flanges, but the contribution from flexural reinforcement of slabs is very marginal. Therefore, for analysis of skeleton RC frames, it is necessary to consider the beneficial effects of RC slabs on CAA capacities.

Appendix 1: Derivation of the compatibility equation

Substituting Equation 5 into Equation 4b, the following equation can be obtained.

$$[\beta l + 0{\cdot}5\varepsilon(1-2\beta)l + (t+t_0)]\sec(\phi+\theta) = \left(\frac{h}{2}-c\right)\tan(\phi+\theta) + \left(\frac{h}{2}-c_1\right)\tan\phi + (1-\varepsilon)\beta l \quad (24)$$

Multiplying both sides of Equation 24 by $\cos(\phi+\theta)$ and rearranging leads to

$$0{\cdot}5\varepsilon l + (t+t_0) = \left(\frac{h}{2}-c\right)\sin(\phi+\theta) + \left(\frac{h}{2}-c_1\right)\tan\phi\cos(\phi+\theta) + (1-\varepsilon)\beta l[\cos(\phi+\theta)-1] \quad (25)$$

As

$$\cos(\phi+\theta) - 1 = -2\sin^2[(\phi+\theta)/2]$$

Equation 25 can be further simplified as

$$0{\cdot}5\varepsilon l + (t+t_0) = \left(\frac{h}{2}-c\right)\sin(\phi+\theta) + \left(\frac{h}{2}-c_1\right)\tan\phi\cos(\phi+\theta) - 2(1-\varepsilon)\beta l\sin^2\left(\frac{\phi+\theta}{2}\right) \quad (26)$$

Dividing both sides of Equation 26 by $\sin(\phi+\theta)$ and rearranging yields

$$c = \frac{h}{2} - \frac{0{\cdot}5\varepsilon l + (t+t_0)}{\sin(\phi+\theta)} + \left(\frac{h}{2}-c_1\right)\frac{\tan\phi}{\tan(\phi+\theta)} - \frac{2(1-\varepsilon)\beta l\sin^2[(\phi+\theta)/2]}{\sin(\phi+\theta)} \quad (27)$$

which is the same as Equation 6.

Since ϕ and θ are small, the trigonometric functions in Equation 6 can be replaced by equivalent infinitesimal mathematical terms. Also, the beam axial strain ε and the movements of the axial restraints $(t+t_0)$ are extremely small compared with l_n. Therefore

$$\sin\theta \approx \theta = M_{u1}/K_r$$

$$\tan(\phi+\theta) \approx (\phi+\theta)$$

$$\tan\phi \approx \phi$$

$$\sin(\phi+\theta) \approx 2\sin\left(\frac{\phi+\theta}{2}\right) \approx \phi+\theta = \frac{\delta}{l_n + 0{\cdot}5\varepsilon b_j + (t+t_0)} \approx \frac{\delta}{l_n} = \frac{\delta}{\beta l}$$

and

$$\phi = \frac{\delta}{\beta l} - \frac{M_{u1}}{K_r}$$

Substituting the above equivalent values of the trigonometric functions into Equation 27 gives

$$c = \frac{h}{2} - \frac{(0{\cdot}5\varepsilon l + t)}{\delta}\beta l - \frac{\beta l t_0}{\delta} + \left(\frac{h}{2} - c_1\right)\left(1 - \frac{M_{u1}\beta l}{K_r \delta}\right) - (1-\varepsilon)\frac{\delta}{2} \quad 28.$$

Substituting $t = N/K_a$ and $\varepsilon = N/E_c A$ into Equation 28 and rearranging yields

$$c = \frac{h}{2} - (1-\varepsilon)\frac{\delta}{2} - \frac{\beta l^2}{2\delta}\left(\frac{1}{E_c A} + \frac{2}{l K_a}\right)N - \frac{\beta l t_0}{\delta} + \left(\frac{h}{2} - c_1\right)\left(1 - \frac{M_{u1}\beta l}{K_r \delta}\right) \quad 29.$$

Compared with unity, the compressive strain ε of beams can be neglected. Therefore, Equation 29 can be simplified as

$$c = \frac{h}{2} - \frac{\delta}{2} - \frac{\beta l^2}{2\delta}\left(\frac{1}{E_c A} + \frac{2}{l K_a}\right)N - \frac{\beta l t_0}{\delta} + \left(\frac{h}{2} - c_1\right)\left(1 - \frac{M_{u1}\beta l}{K_r \delta}\right) \quad 30.$$

which is the same as Equation 8.

Appendix 2: Determination of rotation corresponding to yield moment

The rotation θ_y corresponding to the yield moment M_y at critical sections is determined with the effective stiffness values provided in Table 6-5 of SEI 41-06 (ASCE, 2007). For RC beams, the effective stiffness is $0{\cdot}5E_cI_g$, where E_c is the elastic modulus of concrete and I_g the gross cross-sectional moment of inertia. Typically, the bottom reinforcement in a middle joint is not greater than the top one. Therefore, the middle joint interfaces attain yield moments first. Based on the moment diagram of a two-ends-fixed beam subjected to a point load acting at the beam centre, the counter-flexural point is roughly at the middle point of the 'single-bay' beams. That is, from the counter-flexural point to the middle joint interface (the distance denoted l_{cf}), the curvature increases linearly from zero to ϕ_y. As a result, the yield rotation θ_y is given by

$$\theta_y = \phi_y l_{cf}/2 = (M_y/0{\cdot}5E_cI_g)l_{cf}/2 \quad 31.$$

where the yield moment M_y is determined as (Park and Paulay, 1975)

$$M_y = 0{\cdot}5 f_c bkd(d - kd/3) + f'_s A'_s(d - d') \quad 32.$$

where f_c is the stress of the ultimate compressive concrete fibre, b and d are the width and effective depth of the beam section respectively, f'_s and A'_s are the stress and area of compression steel respectively, d' is the distance from the ultimate compressive fibre of concrete to the centroid of compression steel and k is the ratio of neutral-axis depth to the effective depth, given by

$$k = [(\rho + \rho')^2 n^2 + 2(\rho + \rho' d'/d)n]^{1/2} - (\rho + \rho')n \quad 33.$$

in which ρ and ρ' are the tension and compression reinforcement ratio respectively and n is the ratio of the elastic modulus of steel reinforcement to concrete.

REFERENCES

ACI (American Concrete Institute) (2005) *ACI 318-05: Building Code Requirements for Structural Concrete*. ACI, Farmington Hills, MI, USA.

ASCE (American Society of Civil Engineers) (2007) *SEI 41-06: Seismic Rehabilitation of Existing Buildings*. ASCE, Reston, VA, USA.

FarhangVesali N, Valipour H, Samali B and Foster S (2013) Development of arching action in longitudinally-restrained reinforced concrete beams. *Construction and Building Materials* **47**: 7–19.

GSA (General Services Administration) (2003) *Progressive Collapse Analysis and Design Guidelines for New Federal Office Buildings and Major Modernization Projects*. GSA, Washington, DC, USA.

Guice LK and Rhomberg EJ (1988) Membrane action in partially restrained slabs. *ACI Structural Journal* **85(3)**: 365–373.

MacGregor JG and Wight JK (2005) *Reinforced Concrete Mechanics and Design*, 4th edn in SI units. Prentice Hall, Upper Saddle River, NJ, USA.

Park R and Gamble WL (2000) *Reinforced Concrete Slabs*, 2nd edn. Wiley, Hoboken, NJ, USA.

Park R and Paulay T (1975) *Reinforced Concrete Structures*. Wiley, Hoboken, NJ, USA.

Sasani M, Kazemi A, Sagiroglu S and Forest S (2011) Progressive collapse resistance of an actual 11-story structure subjected to severe initial damage. *Journal of Structural Engineering* **137(9)**: 893–902.

Sasani M and Kropelnicki J (2008) Progressive collapse analysis of an RC structure. *The Structural Design of Tall and Special Buildings* **17(4)**: 757–771.

Sasani M and Sagiroglu S (2008) Progressive collapse resistance

of Hotel San Diego. *Journal of Structural Engineering* **134(3)**: 474–488.

Su YP, Tian Y and Song XS (2009) Progressive collapse resistance of axially-restrained frame beams. *ACI Structural Journal* **106(5)**: 600–607.

US DoD (United States Department of Defense) (2010) *Unified Facilities Criteria (UFC) 4-023-03: Design of Buildings to Resist Progressive Collapse*. US DoD, Arlington, VA, USA.

Yu J and Tan KH (2010) Progressive collapse resistance of RC beam–column sub-assemblages. *Proceedings of 3rd International Conference of Design and Analysis of Protective Structures, Singapore*, pp. 74–83.

Yu J and Tan KH (2013a) Experimental and numerical investigation on progressive collapse resistance of reinforced concrete beam column sub-assemblages. *Engineering Structures* **55**: 90–106.

Yu J and Tan KH (2013b) Structural behaviour of reinforced concrete beam–column sub-assemblages under a middle column removal scenario. *Journal of Structural Engineering* **139(2)**: 233–250.